CrossMark

A microfluidic device for motility and osmolality analysis of zebrafish sperm

Jacob Beckham[1] · Faiz Alam[1] · Victor Omojola[1] · Thomas Scherr[2] · Amy Guitreau[3] · Adam Melvin[4] · Daniel S. Park[5] · Jin-Woo Choi[6] · Terrence R. Tiersch[3] · W. Todd Monroe[1]

Abstract

A microfluidic chip is described that facilitates research and quality control analysis of zebrafish sperm which, due to its miniscule (i.e., 2–5 µl) sample volume and short duration of motility (i.e., <1 min), present a challenge for traditional manual assessment methods. A micromixer molded in polydimethylsiloxane (PDMS) bonded to a glass substrate was used to activate sperm samples by mixing with water, initiated by the user depressing a transfer pipette connected to the chip. Sample flow in the microfluidic viewing chamber was able to be halted within 1 s, allowing for rapid analysis of the sample using established computer-assisted sperm analysis (CASA) methods. Zebrafish sperm cell activation was consistent with manual hand mixing and yielded higher values of motility at earlier time points, as well as more subtle time-dependent trends in motility, than those processed by hand. Sperm activation curves, which indicate sample quality by evaluating percentage and duration of motility at various solution osmolalities, were generated with on-chip microfabricated gold floor electrodes interrogated by impedance spectroscopy. The magnitude of admittance was linearly proportional to osmolality and was not affected by the presence of sperm cells in the vicinity of the electrodes. This device represents a pivotal step in streamlining methods for consistent, rapid assessment of sperm quality for aquatic species. The capability to rapidly activate sperm and consistently measure motility with CASA using the microfluidic device described herein will help improve the reproducibility of studies on sperm and assist development of germplasm repositories.

✉ W. Todd Monroe
tmonroe@lsu.edu

Jacob Beckham
j.e.beckham2@gmail.com

Faiz Alam
fzalam14@gmail.com

Victor Omojola
vomojola3@gatech.edu

Thomas Scherr
thomas.f.scherr@vanderbilt.edu

Amy Guitreau
aguitreau@agcenter.lsu.edu

Adam Melvin
melvin@lsu.edu

Daniel S. Park
spark@lsu.edu

Jin-Woo Choi
choijw@lsu.edu

Terrence R. Tiersch
ttiersch@agcenter.lsu.edu

[1] Department of Biological & Agricultural Engineering, Louisiana State University and Agricultural Center, Baton Rouge, LA, USA

[2] Department of Chemistry, Vanderbilt University, Nashville, TN, USA

[3] Aquatic Germplasm and Genetic Resources Center, Louisiana State University Agricultural Center, Baton Rouge, LA, USA

[4] Cain Department of Chemical Engineering, Louisiana State University, Baton Rouge, LA, USA

[5] Department of Mechanical Engineering, Louisiana State University, Baton Rouge, LA, USA

[6] School of Electrical Engineering & Computer Science, Louisiana State University, Baton Rouge, LA, USA

1 Introduction

Zebrafish (*Danio rerio*) have become a popular vertebrate model organism due to their optically clear embryos, high fecundity, short generation interval, and the ability to apply efficient invertebrate-style genetics to vertebrate-relevant questions (Dooley and Zon 2000; Lieschke and Currie 2007). Their widespread use has resulted in the generation of more than 30,000 research lines (Zebrafish Information Network 2018)), which are costly and inefficient to maintain as live stocks (Hagedorn et al. 2009). As a solution to these complications, cryopreservation of zebrafish gametes is being utilized to reduce the cost of maintaining strains as live populations and provide the opportunities for lines to be shared among research laboratories on demand (Tiersch et al. 2007). In the livestock industry, cryopreservation of sperm has been a widely accepted technology for more than 50 years and supports multibillion global markets for germplasm and genetic resources (Herman 1981). In the case of sperm, pre-freeze and post-thaw quality analyses are essential steps in determining the effectiveness of cryopreservation.

Sperm motility analysis is the current standard for determining sample quality. However, motility analysis of zebrafish sperm is difficult due to the small sample yield for each fish, small cell size, and short motility duration (10–15 s peak initial motility) (Wilson-Leedy and Ingermann 2007; Wolenski and Hart 1987). For externally fertilizing freshwater species such as zebrafish, motility is initiated by introducing the sperm to a hypo-osmotic environment. This drop in osmolality causes the initially dormant sperm to become active. While this activation process has been thoroughly studied (Cosson 2004; Wilson-Leedy and Ingermann 2007; Wilson-Leedy et al. 2009), the exact cascade of events responsible for inducing sperm motility in freshwater fish are still undetermined (Scherr et al. 2015). Motility analysis is performed by first activating the sperm, typically by manual dilution of the sample with water and mixing by hand, followed by visual estimation or use of computer-assisted sperm analysis (CASA) systems (Wilson-Leedy and Ingermann 2007). The ~10 s time lag between activation and analysis, along with inconsistencies in activation due to human variation, are limitations in measuring peak motility of fish sperm, which can result in error-prone evaluation of sperm sample quality. Therefore, there is a need for a platform that enables the rapid mixing and activation of small volumes of zebrafish sperm cells and time sensitive motility analysis, which would allow for standardized methods to be developed across laboratories and repositories.

Microfluidic platforms have the ability to shorten analysis times and reduce the volumes of samples needed. Lab-on-a-chip (LOC) technology has been used in gamete-based studies to sort and orient sperm, (Chen et al. 2013; Cho et al. 2003; Seo et al. 2007) and assess concentration and motility in a variety of species (Chen et al. 2010; Xie et al. 2010). The utility of microfluidics has also been demonstrated in murine *in vitro* fertilization (IVF) technology, where there was an increase in the fertilization rate in microchannels over traditional center-well dishes (Suh et al. 2006). Furthermore, microfluidic devices provide a geometrically constrained microenvironment that is similar to the *in vivo* microenvironment, creating an ideal setting to study the dynamics of sperm and fluid flow interactions (Beebe et al. 2002). To date, only two microfluidic devices have been developed specifically for the activation of zebrafish sperm cells for motility assessment (Park et al. 2012; Scherr et al. 2015), and these do not address osmolality, so this field is relatively open for exploration and new contributions.

Because sperm activation is directly affected by solution osmolality, which is currently measured separately on a separate osmometer instrument, an integrated device capable of on-chip osmometry would aid in discovering the proper protocols for sperm activation and give insight to the physiological mechanisms by which the sperm transition from non-motile to motile. Impedance spectroscopy can be used to characterize the resistance and capacitance of samples by applying an alternating current (AC) input and measuring the magnitude (resistive) and phase (capacitive) components of the resulting signal. The magnitude of admittance, the inverse of the impedance magnitude, is an AC conductivity parameter that can be correlated to the ionic concentration and osmolality of the sample. AC impedance measurements, rather than DC, are preferred in biological media to avoid electrophoresis and electrode fouling. On-chip impedance has proven valuable to detect, for instance, circulating tumor cells (Nwankire et al. 2015) or cell position in a microfluidic channel (Wang et al. 2017).

As such, the goal of our work is to develop simple, inexpensive, and reliable approaches to improve standardization and repeatability of research and support development of community-based germplasm repositories for aquatic species including biomedical models such as zebrafish. The objectives of this study were to develop a microfluidic device with the capabilities to: (1) standardize the method of activation for zebrafish sperm so that all cells in a sample are subjected to similar solution conditions, (2) reproducibly enable motility analysis of the activated sample within 5 s after activation without the interference of bulk fluid movements, and (3) facilitate the generation of sperm activation curves that relate osmolality of the sample solution to duration and percentage of cell motility.

2 Materials and methods

2.1 Device design

The device described herein is a three-inlet microfluidic platform fabricated from polydimethylsiloxane (PDMS) bonded

to a glass substrate with a microfabricated gold floor electrode for osmolality detection (Fig. 1). The device incorporates a form of a monolithic passive micromixer that was previously reported by our group, the Sequential Logarithmic Mixing Apparatus (SeLMA), to standardize the mixing of zebrafish sperm with water by introduction of Dean vortices in the curved channel geometries (Scherr et al. 2012). The prior SeLMA design was modified by widening the sample channel to 200 µm and removing any constrictions in the mixer geometry to reduce the pressure drop within the chip and also prevent channel blockage due to sperm cell entrapment. The mixing efficiency of this design was evaluated, with little differences at the flowrates tested for sperm activation (shown in Supplemental Material). Fluid flow in the device is controlled by using the combination of two components: a simple transfer pipette to induce flow through pneumatic pressure and inlet/outlet reservoirs to balance the fluid flow. The resulting setup allows flow to inexpensively and easily be induced and rapidly halted for accurate CASA readings.

2.2 Device fabrication

AutoCAD (2015 version, AutoDesk, San Rafael, CA) was used to create geometries for the microchannel and electrode designs. A master mold was patterned with SU-8 and fabricated using a single-step photolithography process. SU-8 2025 (MicroChem Corp., Newton, MA) was utilized to create a mold on a mechanical grade 4″ silicon wafer (Universtiywafer.com, South Boston, MA). Protocols from

MicroChem were adapted for the photolithography process (MicroChem 2011). The SU-8 was coated on the silicon wafer using a spin coater (WS-650 Series Spin Processor, Laurell Technologies Corp., North Wales, PA) at 3000 rpm for 30 s to achieve a thickness of 40 µm. The wafer was pre-baked on a hot plate at 65 °C for 5 min and then baked at 95 °C for 15 min with a ramp up of 2 °C/min and gradually cooled down to 25 °C over 2 h. Following baking, the wafer and photomask were positioned on a custom exposure system that utilizes a Blak-Ray B-100 series UV lamp (UVP, LLC, Upland, CA) and exposed to 365 nm UV light with an intensity of approximately 2 mW/cm^2 for 80 s for an effective dose of 160 mJ/cm^2. After exposure, the wafer was baked with the previous ramp up and cool down temperature-time procedure. The wafer was immersed in an SU-8 developer solution (MicroChem Corp., Newton, MA) for 5 min, followed by a fresh developer rinse for 1 min, a last rinse with isopropyl alcohol (Sigma Aldrich, St. Louis, MO) and finally dried with compressed nitrogen gas. To prevent the PDMS from adhering to the master mold, the mold was silanized by adding 2 drops of (tridecafluoro-1,1,2,2,-tetrahydrooctyl)trichlorosilane (Gelest, Morrisville, PA) in a glass petri dish and inserted into a desiccator with the master mold and put under vacuum pressure for 30 min. The master mold was removed and placed on a hotplate and gradually heated to 150 °C for 10 min and allowed to cool to 25 °C over 2 h.

Two electrodes, each 10 µm wide and separated by 10 µm spacing, were fabricated on the glass slide floor of the device by the following lithographic procedures. A chrome-on-glass

Fig. 1 Assembled microfluidic sperm analysis chip. Inset (lower left) shows the modified Sequential Logarithmic Mixing Apparatus (SeLMA) mixer geometry, with constant 200 µm channel width
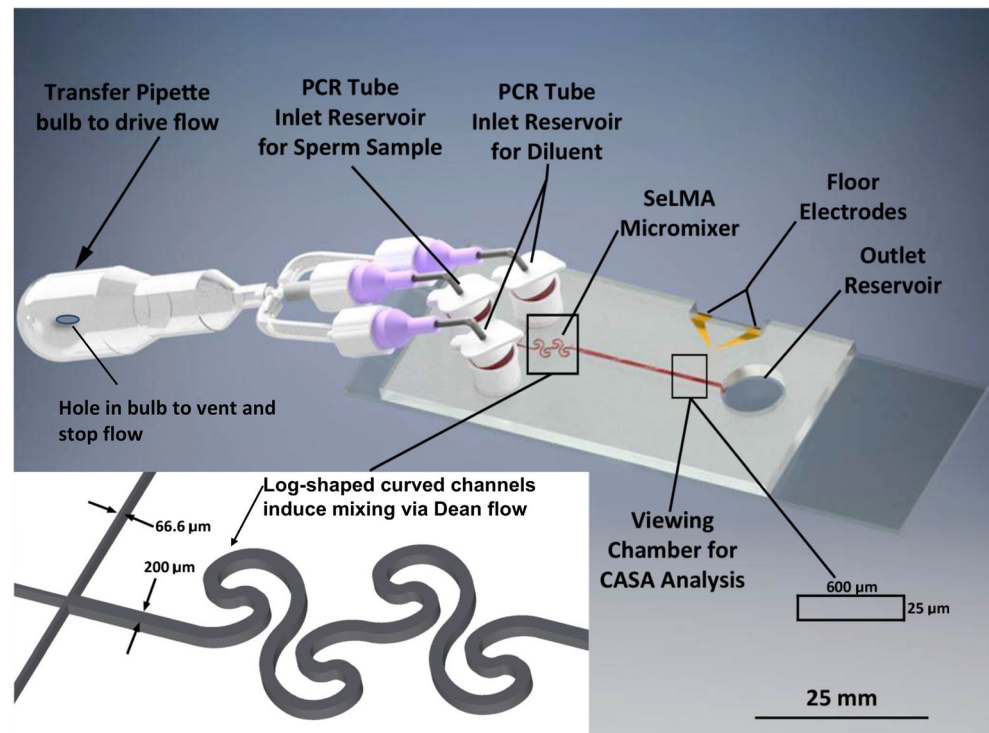
photomask was purchased from Advanced Reproductions (North Andover, MA). Glass slides (75 × 25 mm, Cat#: 3048–002, Thermo Scientific, Waltham, MA) were coated with MICROPOSIT S1813 (Dow Chemical, Midland, MI) positive photoresist using a spin-coater. The photoresist was spin-coated onto the glass slide at 2000 rpm for 60 s. The spin-coated glass slide was baked on a hot plate at 115 °C for 1 min. UV exposure through the optical mask was done at an exposure dose of 40 mJ/cm^2 (UL7000-OBS Exposure Station, Neutronix Quintel, Morgan Hill, CA). The exposed slide was developed in 25% AZ 400 K developer (AZ Electronic Materials, Somerville, NJ) in water for 1 min. Deionized (DI) water refers to water passed through a Millipore Synergy® UV Purification System and dispensed at 18.2 MΩ. The slide was rinsed with DI water and dried with nitrogen, then baked on a hot plate at 115 °C for 1 min. After baking, the sample was cleaned in 100% oxygen plasma using reactive-ion etching at 150 mT at a power of 100 W for 1 min. The sample was coated with 10 nm Cr/100 nm Au using an e-beam evaporator. The sample was immersed in acetone for the lift-off process of the photoresist, resulting in the microelectrodes on glass slides.

The integrated device was molded using traditional soft lithography processes. Briefly, Sylgard 184 polydimethylsiloxane (Dow Corning, Midland, MI) was mixed ratio of 10:1 (base: curing agent) in a weight boat and degassed in a vacuum chamber set to 600 mmHg for 15 min. The PDMS was then poured over a master wafer and cured in an oven at 65 °C for 90 min and removed from the mold. The inlet access holes were created using a 6-mm Harris Uni-core biopsy punch, and the outlet was made using an 8-mm punch. The PDMS device was trimmed and irreversibly bonded to the aforementioned electrode slide after treating in oxygen plasma using a Harric Plasma Cleaner, PDC-32G (Harric Plasma, Ithaca, New York) for 30 s at 1.8 W.

To create the inlet reservoirs, 200 μl microcentrifuge tubes, those commonly used in PCR assays, were cut at the junction of the tapered and non-tapered region, and pneumatic access holes were created by punching through the cap with a sharpened 21 gauge needle (OD 820 μm). The tubes were inserted into the device inlets, and the area around the tubes was sealed with PDMS, and the chip was baked at 65 °C for 90 min. Blunted 1.3 cm, 90° bend, 21 gauge needles were inserted into the pneumatic access holes, which were sealed using clear, waterproof silicone adhesive (P/N: 12045, ITW Consumer, Hartford, CT). The sealant was allowed 24 h to cure. The pneumatic connection was created by using a tubing adaptor that connected a luer-lock needle to 3.2 mm tubing by using a female lure lock attachment on one side and a tubing barb on the other (MTLL230–1, Nordson Medical, Loveland, CO). The adapter was connected to 1/8″ Tygon tubing, which

ran to a 4-way barbed tubing connector (4PX230–1, Nordson Medical, Loveland, CO). The pneumatic driver was fabricated from an 8-mL polypropylene transfer pipette (Samco, Thermo Scientific, Waltham, MA) by creating a hole in the bulb portion of the pipette with an 18 gauge needle (Fig. 1). Squeezing the pipette bulb while the user's finger covered the hole enabled pressurization of sample reservoirs, and removal of the finger permitted rapid depressurization of the system, key to halting flow for CASA analysis as described below.

2.3 Silanization of microchip surfaces

Silanization is a widely applied technique that is used to create a self-assembled monolayer (SAM) using alkoxy- or chlorosilanes with functional head groups to achieve desirable surface properties (Seguin et al. 2010). This technique can be performed on various substrates, such as PDMS, if they have surface hydroxyl groups which, once oxidized, will react with alkoxysilanes to create covalent Si-O-Si bonds. Reports on the silanization of PDMS using 2-[methoxy(polyethyleneoxy)6-9propyl]trimethoxysilane demonstrated its utility in preventing non-specific protein adsorption (Sui et al. 2006), however the effectiveness of this compound to reduce cell fouling on glass (which comprises the floor and most critical transparent surface of the microdevice for cell analysis,) are currently unreported.

The plasma-treated device was subjected to 2-[methoxy(polyethyleneoxy)6-9propyl] trimethoxysilane within 1 min of bonding and left to sit for 15 min. The unreacted silane was removed by flowing DI water into the channel for 5 min and dried by flowing nitrogen gas through the channel until all remaining fluid was evaporated. Contact angle experiments were employed to investigate the surface properties of the silane-treated glass. Clean glass slides were treated using the same procedure used on the microdevice, and the water contact angle was measured in triplicates after a treatment time of 5 min and 15 min using a VCA 2000 contact angle system (VCA, Billerica, MA). To test the cell-repelling characteristics of the silanized microchannels, a side-by-side comparison of treated and non-treated microchannels was performed. Zebrafish sperm samples with a concentration of approximately 1×10^8 cells/mL were introduced into the channel of treated and non-treated devices, and the number of adhered cells was observed with light microscopy.

2.4 Flow rate and cessation analysis

One of the fundamental research themes in microfluidics and LOC technology is the replacement of bulky external equipment with integrated chip-scale technology. Advancement in this area is necessary to further the progress of microfluidics

toward a practical and marketable technology. As a result, equipment-free pumping has become an active area of research that has made possible recent developments in on-chip flow control (Begolo et al. 2014; Glynn et al. 2014; Iwai et al. 2014; Li et al. 2012). As previously discussed, the flow in this device was initiated by completely compressing the transfer pipette bulb by hand, followed by release to de-pressurize the system and halt flow. A small pneumatic regulator (R-7010, Air Logic, Racine, WI) connected between the squeeze bulb and the chip was adjusted to control the maximum amount of pressure applied, which was evaluated at 7, 14 and 21 kPa (1, 2, and 3 PSI, respectively).

Particle tracking velocimetry (PTV) was used to correlate the applied pressure to the flow rate in the chip viewing chamber. To measure flow in the CASA viewing region of the chip, 6 μm polystyrene microparticles (Polysciences, Inc., Warrington, PA) were monitored with video microscopy at 120 frames/s using the MoviePro app (Version 5.2, Depak Sharma) on an iPod Touch (6th generation) (Apple, Cupertino, CA) mounted to the microscope eyepiece using a cell phone mount adapter for eyepieces (Universal Cell Phone Adapter Mount, Gosky Optics, Zheijan Province, China). These videos were segmented into image sequences and thresholded using the Fiji image processing software package (Schindelin et al. 2012; Schneider et al. 2012). The Mosaic 2D/3D Particle Tracker plugin for Fiji was used to find the trajectory of each particle in the image sequence (Sbalzarini and Koumoutsakos 2005). These trajectories were analyzed to find the particle displacement between each frame, which was divided by the time between each frame to find the velocity. For very small particles in flow characterized by a low Reynolds number, the difference between the fluid velocity and the particle velocity can be estimated as:

$$v_p - U = \frac{2}{9}\frac{a^2\left(\rho_p - \rho_f\right)}{\mu}\frac{dv_p}{dt} \qquad (1)$$

where U is the fluid velocity, v_p is the particle velocity, a is the particle radius, ρ_f is the fluid density, ρ_p is the particle density, and μ is the dynamic viscosity (Tropea et al. 2007). Because the density of the polystyrene microparticles (ρ_p) is equivalent to the fluid density (ρ_f), the right side of the equation becomes zero, and the velocities can be considered equal. With this assumption that the microparticles move at the same velocity as the fluid, the average flow rate was found by using the eq. $Q = VA$, where Q is the flow rate, V is the average fluid velocity determined from PTV, and A is the cross sectional area of the microchannel perpendicular to flow. Statistical analyses of flow rates, cessation times, and all other measurements described below were evaluated with a student's t-test, with significance criterion of $P < 0.05$ unless otherwise noted in

other methods below.

2.5 Sperm sample handling and acquisition

Protocols for the use of animals in this study were reviewed and approved by the Louisiana State University Institutional Animal Care and Use Committee (Baton Rouge, LA). Adult zebrafish were obtained from the Zebrafish International Resource Center (ZIRC, University of Oregon, Eugene, USA). Fish were maintained within a 638-L recirculating system. Water quality parameters were maintained at 28 °C, 8.5 pH and 12 h light, 12 h dark photoperiod. Fish were fed to satiation twice daily with a dry food master mix in the morning and *Artemia* (Brine Shrimp Direct, Ogden, Utah) in the afternoon (Zebrafish International Resource Center 2015). Additional water quality parameters that were monitored weekly and kept at an acceptable range included: ammonia (0–1.0 mg/L), nitrites (0–0.8 mg/L) and nitrates (0–15 mg/L). For sperm collection, fish were anesthetized with 0.01% MS-222 (tricaine methanesulfonate, Western Chemical, Inc. Ferndale, WA) and placed ventral side up on a moist sponge and gently stripped. Pooled sperm samples collected from 5 males were diluted with Hanks' balanced salt solution (HBSS: 0.137 M NaCl, 5.4 mM KCl, 1.3 mM CaCl$_2$, 1.0 mM MgSO$_4$, 0.25 mM Na$_2$HPO$_4$, 0.44 mM KH$_2$PO$_4$, 4.2 mM NaHCO$_3$, and 5.55 mM glucose, pH 7.2) at 300 mOsmol/kg to a cell concentration of approximately 1×10^8 cells/ml.

2.6 Comparison of microfluidic and manual sperm activation

As previously stated, the general theme of this device was to standardize zebrafish sperm analysis. This requires elimination of the high variability inherent in manual sperm activation. If the activation performance of the micromixer outweighs that of manual activation methods, it will solve a crucial problem with sperm quality analysis and facilitate the standardization of gamete quality analysis procedures. To validate the utility of the device, it was necessary to compare the motility over time for multiple trials between manual activation performed by a trained technician and on-chip activation in the microfluidic platform. Timelines of the manual and on-chip activation protocols are detailed below.

Manual activation was performed according to established protocols (Yang et al. 2007) by pipetting 1 μL of sperm sample onto the bottom portion of a Makler® Counting Chamber (Irvine Scientific, Santa Ana, CA), followed by addition of 2 μL of DI water. The sperm sample was mixed with the tip of the pipette, and the top of the Makler® Counting Chamber was placed on top. The chamber was placed on the microscope and immediately analyzed by CASA. On-chip

activation was performed by pipetting approximately 60 μL of the same sperm sample solution into the center inlet of the device, and 60 μL of DI water into each side inlet, to give the same 2:1 dilution ratio as manual mixing. The pneumatic bulb was squeezed completely to drive solutions through the micromixer, activating the sample and positioning it in the viewing chamber. Once the presence of sperm were noted in the viewing chamber, removing the user's finger from the bulb hole depressurized the system, halting flow in the viewing chamber for CASA. The HTM-CEROS CASA system (version 14 Build 013, Hamilton Thorne Biosciences, Beverly, Massachusetts, USA) was used to capture 1000 image frames at 60 frames/s. The program settings include a minimum contrast of 50 and minimum cell size of 2 pixels (approximately 5–6 μm). The default values when less than 5 cells were motile were set at 4 pixels for cell size (approximately 10–12 μm) and 65 for cell intensity.

2.7 On-chip osmolality measurements

An initial analysis of impedance signals as a function of osmolality was performed by measuring HBSS at various concentrations in the microfluidic device with a 660B Electrochemical Analyzer (CHI Instruments Inc., Austin, TX). Copper wires (20 gauge) were connected to the pads of floor electrodes with conductive silver epoxy (CircuitWorks Conductive Epoxy, ITW Chemtronics, Kennesaw, GA) and inserted into a tight-fitting pin connector soldered onto the potentiostat leads. The magnitude of admittance from AC impedance signals at 0.01 V amplitude and interrogation frequencies ranging from 1 to 100,000 Hz were compared over HBSS diluted with water from 33 to 305 mOsmol/kg. Because there was greater separation at higher frequencies between admittance values for each osmolality, with a more linear trend (shown in Supplemental Material), all future measurements were carried out at 100,000 Hz.

2.8 On-Chip sperm activation curve measurements

To create an activation curve, the percent activation and motility duration of zebrafish sperm samples were assessed using CASA. Triplicate samples were analyzed at four osmolalities ranging from 100 to 250 mOsm at 50 mOsm increments. The sperm were activated using the on-chip activation methods as described above. The final osmolality of the sample was manipulated by using HBSS dilutions in the diluent reservoirs. The final osmolality was determined by using a freezing point depression osmometer (Osmette III™, Precision Systems Inc.). The osmolality of the sample was monitored via impedance using the on-chip electrode by interrogating the sample in the microdevice.

3 Results and discussion

3.1 Flow rate and cessation analysis

The approximate flow rates of the device at regulated pressures of 7, 14 and 21 kPa (1, 2, and 3 PSI, respectively) were determined by tracking microparticles moving through the device as flow was initiated by squeezing the pipette bulb and then halted by releasing finger pressure. An example of a typical flow rate profile at 14 kPa is shown in Fig. 2a. As expected, when pneumatic pressure was applied to the device, there was a sharp increase in the flow rate followed by a more consistent flow. After the operator's finger was removed from the pipette bulb hole, the depressurization of the system yielded a rapid decrease in flow rate, indicated by the region labeled Δt_{FC} (time required for flow cessation), from approximately 5 μL/min to 0 μL/min over a period of ~0.6 s (Fig. 2a). As expected, some variation in particle velocities was observed prior to chip depressurization, which appeared in a saw tooth pattern (Fig. 2a), likely a result of different particles at different distances from the channel walls having different velocities. The maximum flow rates do not trend linearly (Fig. 2b) with regulated driving pressure as would be predicted by Hagen–Poiseuille flow, likely because the applied pressure from
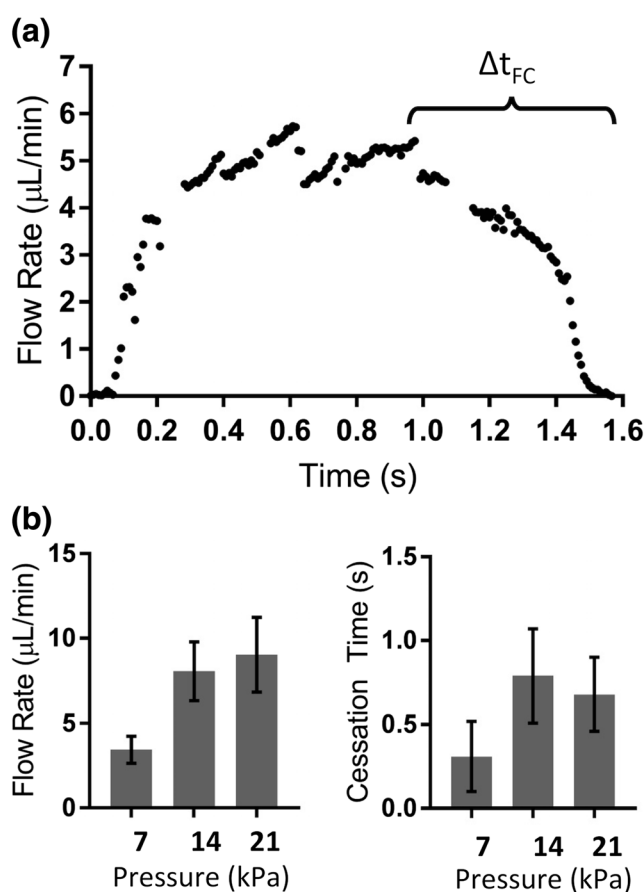
Fig. 2 (**a**): Flow rate profile over time for 14 kPa (2 PSI) as measured using PTV. (**b**): Maximum flow rate (left) and flow cessation time (Δt_{FC}, right) for pneumatically driven microfluidic chip (mean ± std. dev.; $n = 3$)

a single squeeze of the bulb was not sufficient to achieve steady-state state conditions in the microdevice (Bruus 2015).

The flow cessation times at all driving pressures were not statistically different from each other ($P < 0.05$). In part, due to the hole in the pipette bulb that allows rapid depressurization, the lack of pressure drop causing constrictions in the mixer of the chip, and also the relatively large 8-mm diameter waste reservoir of the chip, no back flow was observed in any trials. The aforementioned design features were included to reduce back flow, which occured in the initial development of the device and produced artifact in CASA measurements. The short flow cessation times represent a substantial and highly practical improvement over the previous reported devices (Park et al. 2012; Scherr et al. 2015), which required 7–10 s to achieve flow cessation. Halting flow rapidly in the microdevice enables the user to analyze zebrafish sperm quality directly after activation, thus ensuring that analyses can be accurately performed during the initial ~10 s peak motility phase of zebrafish sperm activation.

3.2 Silanization of microchip surfaces

Silanized glass slides showed water contact angles that decreased from $24.10 \pm 0.76°$ for native glass to $13.68 \pm 3.09°$ after a treatment time of 5 min, and decreased further to $6.68 \pm 1.74°$ after a treatment time of 15 min. The decrease in water contact angle indicates that the hydrophobicity of the glass decreased after treatment with the silane, consistent with the formation of a hydrophilic layer. Correspondingly, there was an decrease in cell adhesion observed in the treated device compared to the untreated devices, with 500 ± 50 adhered cells in the viewing chamber of the untreated device versus an average of 12 ± 3 cells adhered in the treated devices (Supplemental Material includes video microscopy comparisons of cell adhesion). These results indicate that treating the microchannel with the silane reduced the adhesion of zebrafish sperm; thus silanized devices were used in all subsequent experiments.

3.3 Comparison of manual and microfluidic sperm activation

The activation of zebrafish sperm by traditional manual mixing methods was compared to on-chip activation in the microdevice with the same sample solution diluted 2:1 (water:sperm) at various time points (Fig. 3). At the earliest measurable time point common to both systems, 3 s following activation, on-chip activation resulted in $63 \pm 2\%$ motility, not significantly different from manual activation by an experienced technician of $58 \pm 10\%$, ($P = 0.59$). The variation in motility from manual activation would likely be higher with novice workers. The smaller variability in motility from on-chip activation is likely due to the more consistent mixing of sperm and water, and more controlled flow conditions (e.g.,

Fig. 3 (Top) Protocol and timeline of manual versus on-chip activation of zebrafish sperm for motility analysis. (Bottom) Comparison of manual (grey striped bars) and on-chip (black bars) activation over time (mean ± std. dev.; n=3). * Indicates significant difference ($P < 0.05$)
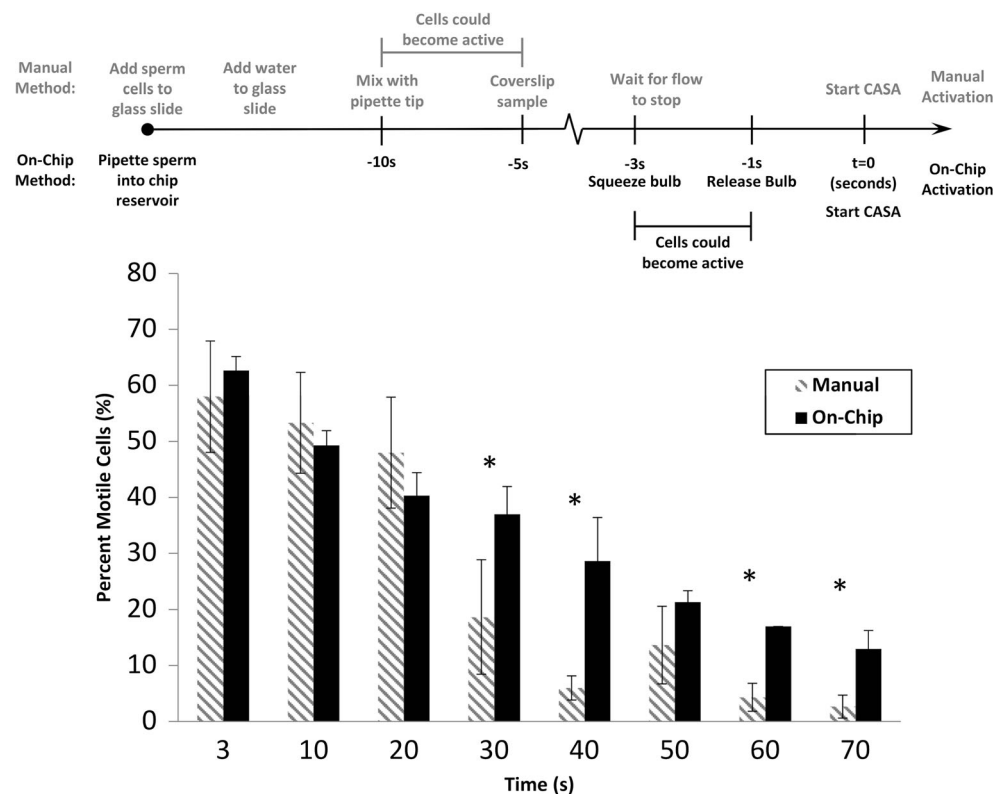
lack of turbulence, more rapid flow cessation) offered in the microfluidic device. Measurements of initial motility with the manual approach also require significant user skill in rapidly and thoroughly mixing the sample, placing a coverslip over it, and choosing the earliest time point where bulk fluid flow is stopped for an accurate motility assessment with CASA. Shear stresses on the sperm cells could be different in manual versus on-chip activation methods and could contribute to potential damage of tails and cell bodies.

While not measured in this study, shear stresses are likely be more variable in the manual method, where different dispensing flowrates from the user's pipetting technique are likely subject to greater variability than the flowrates observed with the microdevice. As mentioned in Section 2.1, the constriction present in earlier versions of the SeLMA micromixer (Park et al. 2012; Scherr et al. 2015) were removed to reduce the pressure drop within this chip, which also reduced the concentrated points of highest shear along the sample path. No shearing of sperm cells was observed in either the manual or on-chip methods tested, and, because the initial motilities measured in the two methods were similar as noted above, it is unlikely that the on-chip micromixer caused damage to sperm cells. The silanization of chip surfaces prevented cell adhesion in this device, which also lessened the likelihood of cell aggregation, particularly at the micromixer constrictions, observed in those prior studies.

The on-chip motility analysis did reveal time-dependent differences in motility that were not observed with manual activation. For example, on-chip motility at 3 s ($63 \pm 2\%$) dropped significantly at 10 s ($49 \pm 3\%$, $P = 0.006$), whereas at these same time points, the manual method only dropped from $58 \pm 10\%$ to $53 \pm 9\%$. Differences in motility levels were also observed between the two systems at longer time points following activation: 40 s ($P = 0.02$), 60 s ($P = 0.002$), and 70 s ($P = 0.02$), where the manually activated sperm had a greater decline in motility compared to on-chip activated sperm. The microdevice thus shows promise in enabling studies over longer durations, where differences in sample quality could be more easily discerned at either earlier time points (initial motility) or later time points (where either cellular energy stores are consumed earlier or cellular damage accumulates in lesser quality samples, leading to a sharper decline in motility). This approach is also an improvement over the other reported microfluidic devices for aquatic sperm cell activation (Park et al. 2012; Scherr et al. 2015). The current system does not require syringe pumps to initiate flow or off-chip solenoid valves to stop flow prior to initiation of CASA.

3.4 On-Chip measurement of osmolality

In addition to sperm motility analysis, the integrated device was designed to determine on-chip osmolality of the sperm sample via impedance measurements. To create a standard curve, impedance analysis was performed on dilutions of HBSS ranging from 33 to 305 mOsmol/kg. The magnitude of admittance, the

inverse of the impedance magnitude, was found to linearly increase with osmolality from 0.04 ± 0.003 to 0.2 ± 0.006 mS (Fig. 4a). This was expected, as the conductivity of the solution should increase (thus decreasing the resistance) with increasing concentration of ions at higher osmolalities. There was low variability in impedance signals observed between all tests (<1° and < 100 Ω). However, each device was individually calibrated to ensure accuracy due to small variations between the microfabricated electrodes that arose, including variation in metal deposition during sputtering, different amounts of silver epoxy applied, and small changes in contact area when electrodes were connected and disconnected from the potentiostat.

The osmolality of sperm cell solutions at the standard concentration of 1×10^8 cells/mL and varying osmolality were interrogated to determine if the presence of cells in the electrode region of the microdevice affected measurements. The admittance magnitude values showed a higher variability at

(a)

(b)
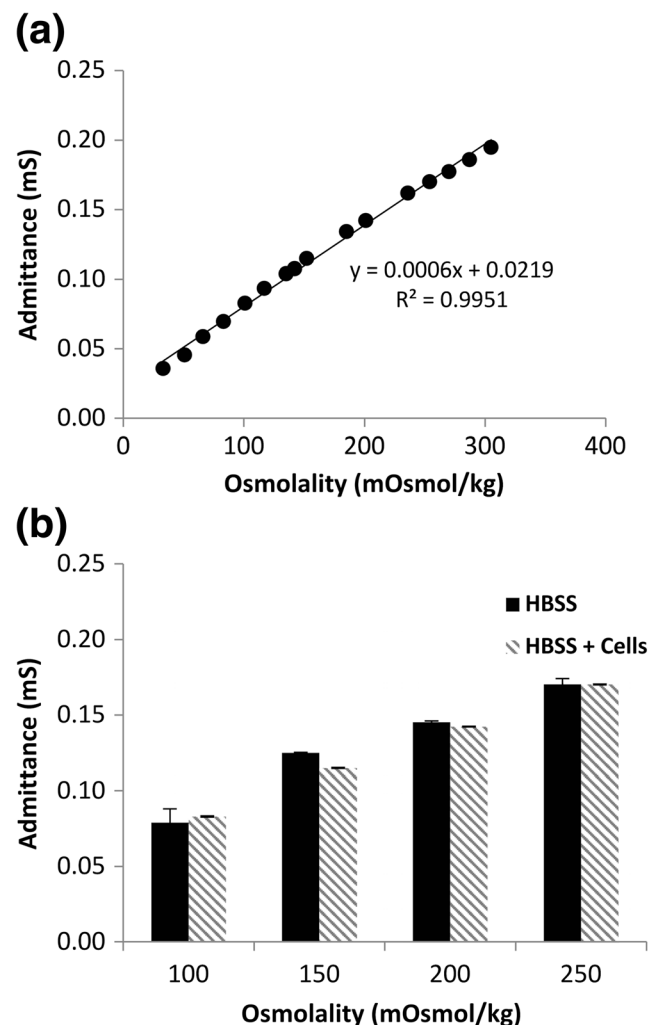
Fig. 4 (a): Standard curve for on-chip osmolality determination using the magnitude of admittance from impedance spectroscopy at 100kHz (mean ± std. dev.; n=3). (b): Effect of sperm samples in the chip interrogation region on impedance signals (grey striped bars) compared to HBSS alone (black bars) (mean ± std. dev.; $n = 3$)

100 mOsmol/kg (±0.0025 mS) during the experiments with sperm, but this was not observed at other osmolalities tested (Fig. 4b). There was no significant difference in the sensor response when cells were present other than at 150 mOsmol/kg. Due to the higher variability of admittance at the lower (100 mOsmol/kg) range, the osmolality uncertainty was ±14 mOsmol/kg; this uncertainty decreased to ±7 mOsmol/kg at the higher (250 mOsmol/kg) end of the practical sensor range for sperm solution measurements (Fig. 4b). The larger variability and potential for interference at these lower ranges of osmolality suggest that further optimization of electrode size and spacing might improve sensor performance. For example, increasing electrode spacing would presumably interrogate a larger volume of solution that would have a larger signal of admittance magnitude, providing more sensitivity, yet might also be subject to artifact by the greater likelihood of cells (or debris) being present in the interrogation area. Despite this, the sensor was deemed appropriate for determining osmolality in the range of typical sperm activation curves, detailed below.

3.5 On-Chip sperm activation curve measurements

Assessment of sample osmolality within the microchannel would facilitate the generation of sperm activation curves used to determine the relationships between osmolality and sperm motility. Sperm activation percentage as a function of osmolality will aid in ensuring proper protocols for sperm activation and give insight to the physiological mechanisms by which the sperm transition from non-motile to motile. On-chip activation and motility was investigated at osmolalities of 100–250 mOsmol/kg. This range was chosen for its biological relevance and the fact that in the current 3-inlet design, it is the lowest range that can be generated without prematurely activating the sample, where the cell suspension is at 300 mOsmol/kg and the adjacent diluent channels could be, at a minimum, negligible osmolality. As expected, the percent of motile sperm cells decreased as the osmolality of the final solution was increased (Fig. 5a). As the osmolality was increased from 100 to 200 mOsmol/kg, the progressive motility decreased from $62 \pm 6\%$ to $38 \pm 8\%$. At 250 mOsmol/kg, the motility dropped to 3%, which was consistent with previous reports on zebrafish sperm motility (Yang et al. 2007). The increase in the osmotic pressure of the cell solution also resulted in changes of how long motile sperm cells continued to swim (Fig. 5b). The motility duration increased from 67 ± 6 s to 128 ± 12 s as the final osmolality increased from 100 to 200 mOsmol/kg. This result from the microfluidic platform was also consistent with previous reports accomplished via manual mixing (Yang et al. 2007). In future developments of microchip devices, different dilutions could be created on-chip by adjusting the flow between sperm and diluent, or by using HBSS in diluent sample inlets, or incorporating dilution arrays
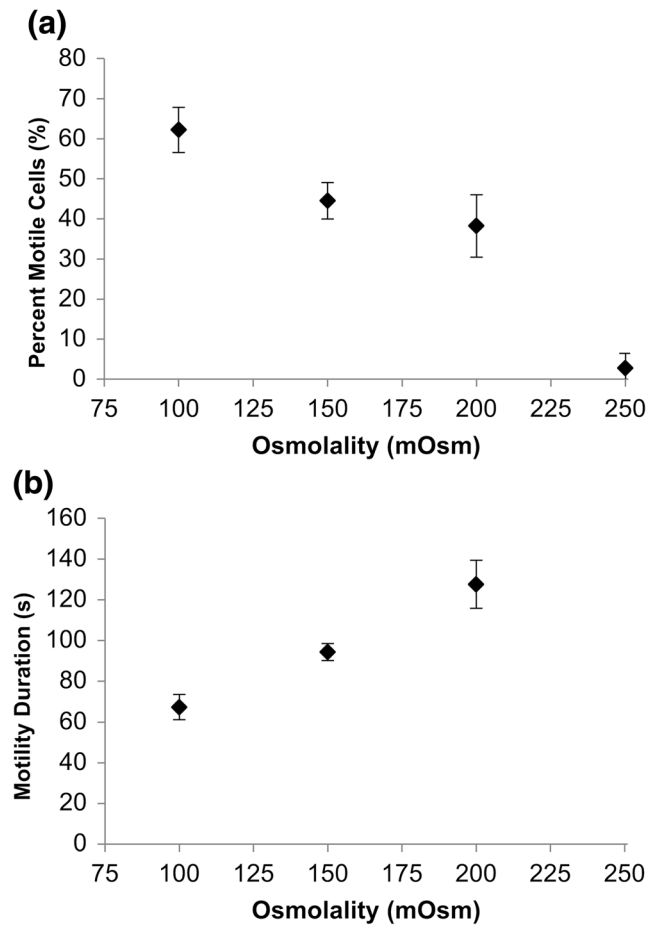
Fig. 5 Zebrafish sperm activation curves measured on-chip. (**a**): percentage of motile zebrafish sperm activated at various osmolalities of diluted HBSS; (**b**): motility duration of active sperm at various osmolalities of diluted HBSS (mean ± std. dev.; $n = 3$)

of various geometries (Sugiura et al. 2010) that could enable several osmolalities to be evaluated in parallel on-chip.

4 Conclusions

In this study, a microfluidic device designed to activate zebrafish sperm for motility analysis and to measure the osmolality of the cell solution in the microchannel was introduced. The on-chip micromixer enabled reproducible mixing of fluids, which resulted in consistent zebrafish sperm cell activation. The incorporation of the micromixer removed the potential of human error associated with hand mixing, leading to standardization of activation techniques. The incorporation of a simple, pneumatically driven, flow controller in place of a syringe pump facilitated a flow cessation time of ~1 s for all pressures tested. This is a 5-fold improvement over previous microfluidic devices used for zebrafish sperm analysis, which had latent periods of 7–10 s after activation before bulk fluid flow subsided (Park et al. 2012; Scherr et al. 2015). More importantly, prompt cessation of flow allowed for motility analyses to be performed reliably

during the initial peak motility phase of activation, thereby ensuring this parameter to be collected, which may prove to be a more useful indicator of sample quality. This represents an improvement over manual activation methods, which can have a latency period of ~10 s due to procedural requirements and human variability. On-chip activation and analysis revealed a sharp decrease in motility within this 10 s period that could not be observed with the manual activation method.

This equipment-free solution to flow control also facilitated replacement of syringe pumps, often used to drive flow in microdevices, with a simple pressure-driven system comprised of common laboratory pipettes and microcentrifuge tubes. This design change decreased the volume of the zebrafish sperm sample needed for analysis from ~200 μL of diluted sample to ~60 μL, which could be further decreased with optimization of sample reservoir geometry. The present study focused on zebrafish as a research model because of their global importance in biomedical research and routine availability of sperm samples. However, these fish produce miniscule volumes of sperm (2–5 μL prior to a 25 to 40-fold dilution, yielding a working concentration of $\sim 5 \times 10^8$ cell/mL) (Yang et al. 2007), and samples from multiple males are often pooled to provide enough volume for analysing sperm properties. If zebrafish samples from a single fish were to be analysed, the existing design could accommodate a smaller sperm sample loaded into the device followed by a moderate volume of a biocompatible immiscible fluid (e.g. Fluorinert fluorocarbon, 3M, Maplewood, MN) to ensure consistent loading into the channel. It is worth noting that sperm activation analysis is relevant to any species being studied for cryopreservation, and most commercially relevant large-bodied species such as carp, catfish, trout, and salmon all provide much larger sperm samples due to a of high sperm density in the testis (e.g.,$\sim 10^{10}$ cells/mL), often yielding greater than 100 mL of sperm sample per fish after dilution (Tiersch 2011), providing more than ample volume for activation analyses.

The on-chip microelectrode permitted the measurement of the osmolality of a zebrafish sperm sample in the device channel. The capability to measure osmolality on-chip permits the researcher to analyse the osmolality of a sample in real time, which saves time and facilitates the creation of accurate activation curves on-chip. While the current system utilized a laboratory-grade potentiostat for impedance analysis, precise and portable devices are being developed (Dryden and Wheeler 2015; Rowe et al. 2011) which could reduce cost, complexity, and bulk, thus increasing likelihood of use in biological laboratories.

Overall, the device described herein has the potential to aid in the standardization of cryopreservation techniques for zebrafish sperm by reducing the error caused by the human element in experiments involving the investigation sperm motility and osmolality. Aquatic species have emerged as a dominant alternative to mammalian models for biomedical research. Current NIH support of Zebrafish research alone is approximately 900 projects totalling $451,000,000 (National Institutes of Health 2018). Essentially all of this research is based on the reliable availability of specific lines of zebrafish. Such lines are typically maintained as live animals at great cost and substantial risk, and, recently, major stock centers have begun line maintenance based on sperm cryopreservation (Torres and Tiersch 2018). This technology is currently not standardized and makes these valuable research resources vulnerable to loss. The standardization of motility analysis techniques, such as those that could come from the device described herein, could reduce the ambiguity in data generated by manual activation methods across research laboratories and germplasm repositories.

References

D.J. Beebe et al., Annu. Rev. Biomed. Eng. **4**, 261–286 (2002). https://doi.org/10.1146/annurev.bioeng.4.112601.125916

S. Begolo et al., Lab Chip (2014). https://doi.org/10.1039/c4lc00910j

Bruus, H., in *Microscale Acoustofluidics*, ed. By T. L. Laurell, Andreas (The Royal Society of Chemistry, 2015), 1-28

Y.-A. Chen et al., Microfluid. Nanofluid. **10**, 59–67 (2010). https://doi.org/10.1007/s10404-010-0646-8

C.Y. Chen et al., Analyst **138**, 4967–4974 (2013). https://doi.org/10.1039/c3an00900a

B.S. Cho et al., Anal. Chem. **75**, 1671–1675 (2003). https://doi.org/10.1021/ac020579e

J. Cosson, Aquac. Int. **12**, 69–85 (2004)

K. Dooley, L.I. Zon, Curr. Opin. Genet. Dev. **10**, 252–256 (2000). https://doi.org/10.1016/S0959-437X(00)00074-5

M.D. Dryden, A.R. Wheeler, PLoS One **10**, e0140349 (2015). https://doi.org/10.1371/journal.pone.0140349

M.T. Glynn et al., Lab Chip **14**, 2844–2851 (2014). https://doi.org/10.1039/c4lc00264d

M. Hagedorn et al., Cryobiology **58**, 12–19 (2009). https://doi.org/10.1016/j.cryobiol.2008.09.013

H. A. Herman, *Improving cattle by the millions. NAAB and the development and worldwide application of artificial insemination*, 1st Edition, (University of Missouri Press, Columbia, 1981)

K. Iwai et al., Lab Chip **14**, 3790–3799 (2014). https://doi.org/10.1039/c4lc00500g

W. Li et al., Lab Chip **12**, 1587–1590 (2012). https://doi.org/10.1039/c2lc40125h

G.J. Lieschke, P.D. Currie, Nat. Rev. Genet. **8**, 353–367 (2007). https://doi.org/10.1038/nrg2091

MicroChem, Permanent Epoxy Negative Photoresist Processing Guidelines for SU-2025. (MicroChem, 2011), http://microchem.

com/pdf/SU-82000DataSheet2025thru2075Ver4.pdf. Accessed May 12, 2013

National Institutes of Health, Research Portfolio Online Reporting Tools. (National Institutes of Health, Bethesda, MD, 2018), https://report.nih.gov. Accessed May 5, 2018

C.E. Nwankire et al., Biosens. Bioelectron. **68**, 382–389 (2015). https://doi.org/10.1016/j.bios.2014.12.049

D.S. Park et al., Theriogenology **78**, 334–344 (2012). https://doi.org/10.1016/j.theriogenology.2012.02.008

A.A. Rowe et al., PLoS One **6**, e23783 (2011). https://doi.org/10.1371/journal.pone.0023783

I.F. Sbalzarini, P. Koumoutsakos, J. Struct. Biol. **151**, 182–195 (2005). https://doi.org/10.1016/j.jsb.2005.06.002

T. Scherr et al., J. Micromech. Microeng. **22**, 55019 (2012). https://doi.org/10.1088/0960-1317/22/5/055019

T. Scherr et al., Biomed. Microdevices **17**, 65 (2015). https://doi.org/10.1007/s10544-015-9957-6

J. Schindelin et al., Nat. Methods **9**, 676–682 (2012). https://doi.org/10.1038/nmeth.2019

C.A. Schneider et al., Nat. Methods **9**, 671–675 (2012)

C. Seguin et al., Appl. Surf. Sci. **256**, 2524–2531 (2010). https://doi.org/10.1016/j.apsusc.2009.10.099

D.B. Seo et al., Microfluid. Nanofluid. **3**, 561–570 (2007). https://doi.org/10.1007/s10404-006-0142-3

S. Sugiura et al., Anal. Chem. **82**, 8278–8282 (2010). https://doi.org/10.1021/ac1017666

R.S. Suh et al., Hum. Reprod. **21**, 477–483 (2006). https://doi.org/10.1093/humrep/dei323

G. Sui et al., Anal. Chem. **78**, 5543–5551 (2006). https://doi.org/10.1021/ac060605z

T.R. Tiersch, C.C. Green *Cryopreservation in Aquatic Species*, 2nd edition. World Aquaculture Society, Advances in World Aquaculture, Baton Rouge, Louisiana, 1003 pages (2011)

T.R. Tiersch et al., Soc. Reprod. Fertil. Suppl. **65**, 493–508 (2007)

L. Torres, T.R. Tiersch, J. World Aquacult. Soc. (In Press) (2018). https://doi.org/10.1111/jwas.12541

C. Tropea et al., *Springer handbook of experimental fluid mechanics*, 1st Edition, (Springer Science & Business Media, Berlin, 2007)

H. Wang et al., Lab Chip **17**, 1264–1269 (2017). https://doi.org/10.1039/c6lc01223j

J.G. Wilson-Leedy, R.L. Ingermann, Theriogenology **67**, 661–672 (2007). https://doi.org/10.1016/j.theriogenology.2006.10.003

J.G. Wilson-Leedy et al., Theriogenology **71**, 1054–1062 (2009). https://doi.org/10.1016/j.theriogenology.2008.11.006

J.S. Wolenski, N.H. Hart, J. Exp. Zool. **243**, 259–273 (1987)

L. Xie et al., Clin. Chem. **56**, 1270–1278 (2010). https://doi.org/10.1373/clinchem.2010.146902

H. Yang et al., Theriogenology **68**, 128–136 (2007). https://doi.org/10.1016/j.theriogenology.2007.02.015

Zebrafish Information Network (ZFIN). (University of Oregon, Eugene, 2018), http://zfin.org/. Accessed May 5, 2018

Zebrafish International Resource Center, Dry Food Recipe for fish 90+ dpf. (University of Oregon, 2015), http://zebrafish.org/documents/protocols/pdf/Fish_Feeding/Flake_Food/Dry_Food_Recipes2015.pdf. Accessed May 10, 2015